Özgür Ergül
Department of Electrical and Electronics Engineering
Middle East Technical University
TR-06800, Ankara, Turkey
E-mail: ozergul@metu.edu.tr

SOLBOX-12

Hande İbili, Barışcan Karaosmanoğlu, and Özgür Ergül

Department of Electrical and Electronics Engineering
Middle East Technical University
TR-06800, Ankara, Turkey
E-mail: ozergul@metu.edu.tr

1. Introduction

In three-dimensional electromagnetic solvers, extreme values for electrical parameters typically lead to instability, inaccuracy, and/or inefficiency issues. Despite using the term "extreme," such relatively large or small values of conductivity, permittivity, permeability, wavenumber, intrinsic impedance, and other electrical parameters are commonly observed in natural cases. Computational electromagnetic solvers adapt themselves to handle challenging cases by replacing exact models with approximate models, while minimizing the modeling error due to these transformations. For example, most metals with high conductivity values are assumed to be perfectly conducting, especially if the considered structure is comparable to the wavelength. This is very common for practical devices, such as antennas, metamaterials, filters, etc., at radio and microwave frequencies. In some cases – e.g., when the overall structure is small in terms of a wavelength – even a full-wave solver may not be required to analyze the underlying phenomena. Examples are circuit theory based on lumped elements and transmission-line modeling. On the other side, penetrable models are commonly used to represent dielectric and magnetic materials, when their electrical parameters (specifically, permittivity and permeability) have numerically "reasonable" values that facilitate their full-wave solutions without a fundamental issue. As the electrical parameters become extreme and other conditions (sizes, excitations, geometric properties) are satisfied, numerical approximations may again become useful, leading to the well-known implementations such as those based on impedance boundary conditions and physical optics.

New structures and devices in the state-of-the-art technology often require very accurate simulations with extreme values for electromagnetic parameters. One well-known regime involves the plasmonic behaviors of some metals at optical frequencies [1]. In the frequency domain, traditional solvers can be extended to accurately handle such exotic cases by employing complex permittivity values with negative real parts [2-13]. As the frequency drops, the real part of the permittivity is increasingly negative (becoming extreme), while it becomes unnecessary to enforce the plasmonic modeling (and hence to use extreme permittivity values) due to quickly decaying waves inside objects. Nevertheless, there is no obvious boundary between plasmonic modeling and perfectly conducting (limit) modeling and, more importantly, a suitable model at a given frequency may actually depend on the structure and the considered application [14]. Similar issues occur when dealing with detailed metallic structures, such as circuits when the skin effect cannot be ignored and metallic losses must be included (even if they are large) in

their electromagnetic analysis [15]. In all these cases, we obviously need very reliable numerical solvers based on generalized formulations and algorithms that automatically converge into suitable forms for given conditions without externally enforcing risky approximations described above.

However, what happens when extreme electrical parameters must be fully included in an electromagnetic analysis? In the context of the surface integral equations in the frequency domain, the wavenumber that contains medium parameters is used in the Green's function, i.e., the kernel of the equations. The value of the wavenumber hence determines how fast the Green's function decays and how much it is oscillatory. These properties should be considered together with the interaction distances that depend on the metric size of the structure under investigation. However, even when the wavenumber is well balanced with metric distances such that numerical issues do not arise from the Green's function itself, absolute values of permittivity, permeability, and/or their ratio as the intrinsic impedance, may strongly affect the stability of solutions. This is because integral-equation (and similar) formulations are mostly designed (for example, numerically balanced) for reasonable values of these quantities [16].

In this issue of Solution Box, a set of frequency-domain scattering problems involving spherical particles is presented. Neither the geometry nor the size in terms of wavelength is the challenge in these problems. Instead, some hypothetically extreme values for the permittivity are considered, such that numerical issues may arise in the conventional solvers. Sample solutions using a specialized integral-equation formulation are also presented as references for candidate solutions by using other implementations developed by the readers. As usual, we are looking for alternative solutions, which are probably more accurate, stable, and/or efficient than presented here. Please also consider sending your solutions for the earlier problems (SOLBOX-01 to SOLBOX-11) to present your work in this column.

2. Problems

2.1 Problem SOLBOX-12 (by Hande *İbili, Barışcan Karaosmanoğlu, and Özgür Ergül*)

The SOLBOX-12 problem includes scattering problems involving spherical particles of diameter 1.0 μm at 10 THz and 1 THz, i.e., when the diameter was $\lambda/30$ and $\lambda/300$ where λ was the wavelength in vacuum. Each sphere was located at the origin (in vacuum) and illuminated by a plane wave (1 V/m) propagating in the z direction. For numerical solutions with surface integral equations, discretization was applied by using 50 nm triangles for 10 THz and 30 nm triangles for 1 THz, leading to totals of 2720 and 7722 triangles, respectively. For the relative complex permittivity of the sphere in the frequency domain, the following hypothetical values were considered:

Positive real part: (20000+2i), (20000+200i), (20000+20000i), (2+20000i), (200+20000i)

Negative real part: (–20000+2i), (–20000+200i), (–20000+20000i), (–2+20000i), (–200+20000i)

As a remarkable example, the relative complex permittivity values for pure silver at 10 THz and 1 THz are approximately (–17000+20000i) and (–30000 + 340000i) , respectively, so that the values above were not simply academic trials. As the results of simulations, scattering characteristics (e.g., equivalent currents, near-zone fields, and/or far-zone fields) were required to be found.

3. Solution to Problem SOLBOX-12

3.1 Solution Summary

Solver type (e.g., noncommercial, commercial): Noncommercial research-based code developed at CEMMETU, Ankara, Turkey

Solution core algorithm or method: Frequency-domain Method of Moments

Programming language or environment (if applicable): *MATLAB + MEX*

Computer properties and used resources: 2.5 GHz Intel Xeon E5-2680v3 processors (using single core)

Total time required to produce the results shown Total time required to produce the results shown (categories: < 1 sec, < 10 sec, < 1 min, < 10 min, < 1 hour, < 10 hours, < 1 day, < 10 days, > 10 days): < 1 hour for each problem

3.2 Short Description of the Numerical Solutions

The scattering problems listed under SOLBOX-12 were solved by using an iterative Method of Moments. The problems were formulated with a modified combined tangential formulation (MCTF) [17] that was known to be stable for large (and particularly negative) permittivity values. The MCTF was discretized by using the Rao-Wilton-Glisson (RWG) functions. Electromagnetic interactions (matrix elements) were computed via Gaussian quadrature formulas combined with standard singularity-extraction methods. All solutions were performed by using the Generalized Minimal Residual (GMRES) method, while the target residual error was selected as 0.0001.

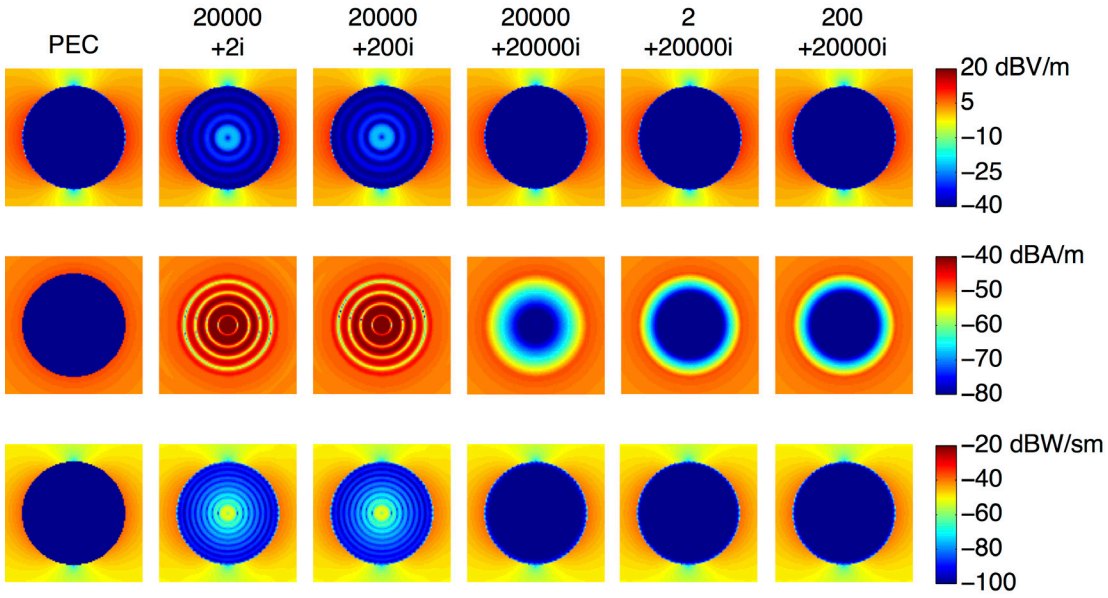

Figure 1. The solutions of the scattering problems (SOLBOX-12) involving spheres with positive values for the real part of the relative permittivity (values are shown on the top) at 10 THz. The electric-field intensity (first row), the magnetic-field intensity (second row), and the power density (third row) were plotted in the vicinity of the spheres.

3.3 Results

Figure 1 presents the results for the scattering problems involving the spheres with positive real permittivity values. As an additional solution, we also considered the case of a perfectly electrically conducting (PEC) sphere. The electric field intensity (first row), the magnetic field intensity (second row), and the power density (third row) were plotted in the vicinities of the spheres on the cross-sectional (x-y) plane. The dynamic ranges were $[-40, 20]$ dBV/m, $[-80, = 40]$ dBA/m, and $[-100, -20]$ dBW/sm, respectively (also for the other results). Despite that the outer intensity and density values were similar to each other for different cases (permittivity values), the internal quantities were quite different from each other. We also had the following observations:

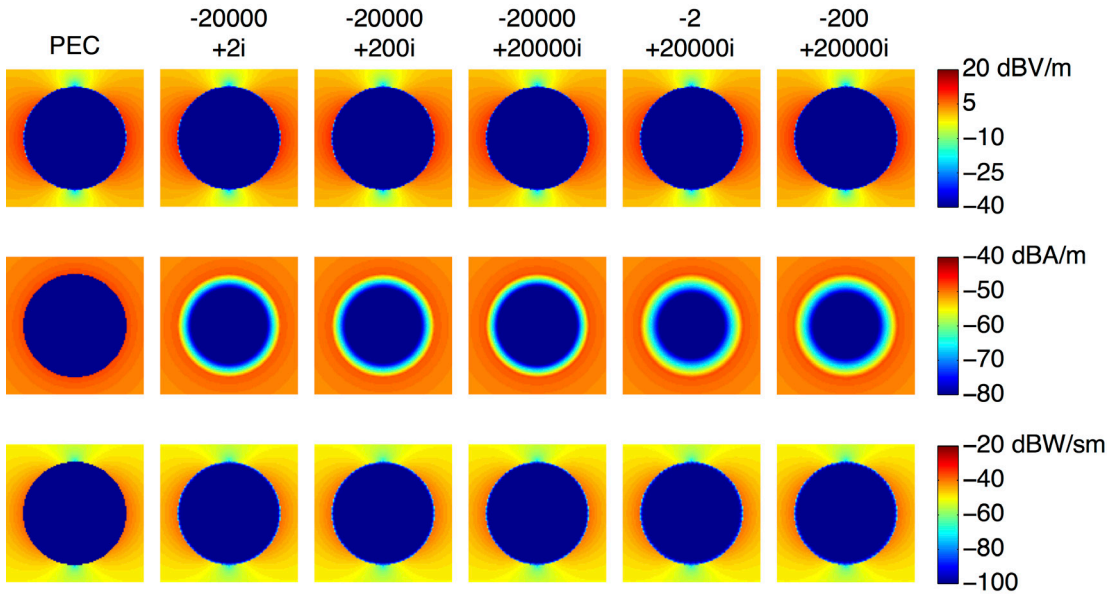

Figure 2. The solutions of the scattering problems (SOLBOX-12) involving spheres with negative values for the real part of the relative permittivity (values shown on the top) at 10 THz. The electric-field intensity (first row), the magnetic-field intensity (second row), and the power density (third row) were plotted in the vicinity of the spheres.

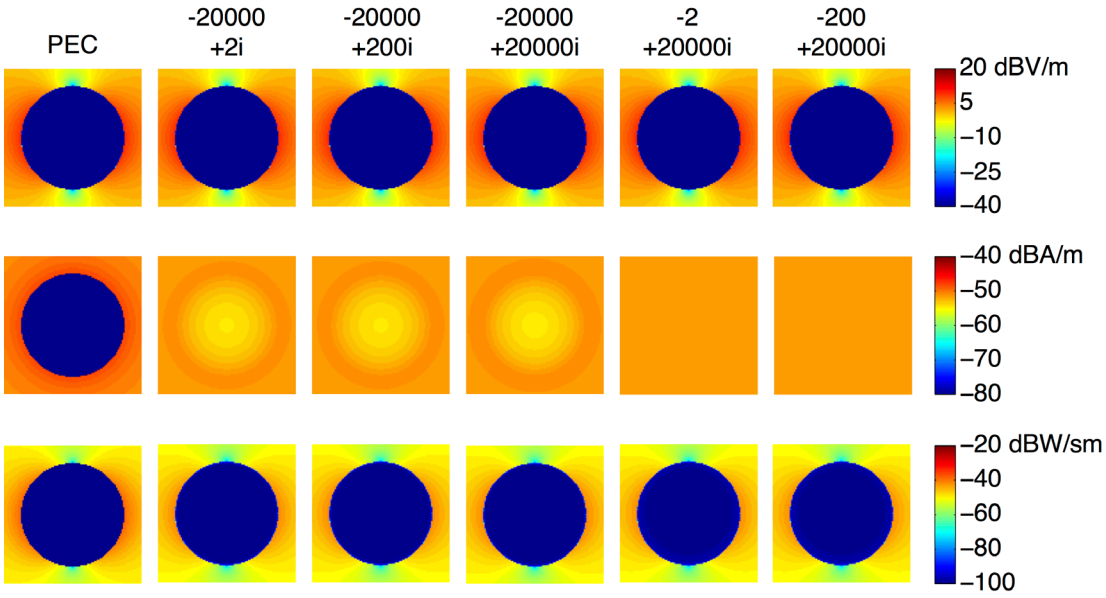

Figure 3. The solutions of the scattering problems (SOLBOX-12) involving spheres with negative values for the real part of the relative permittivity (shown on the top) at 1 THz. The electric-field intensity (first row), the magnetic-field intensity (second row), and the power density (third row) were plotted in the vicinity of the spheres.

For all cases, the electric-field intensity was relatively small inside the spheres. This was as opposed to the behaviors of the magnetic-field intensity and the power density, which were particularly large in the first two cases (20000+2i and 20000+200i). Here, "large" and "small" are defined by considering outer fields.

In the first two cases, oscillatory behaviors were also observed in the intensity and density distributions, which seemed to be related to the relatively large values for the real part of the wavenumber. On the other side, for the last three cases, decaying characteristics were mainly observed due to the large values for the imaginary part of the wavenumber. Nevertheless, even for the relative permittivity of (200+20000i), a remarkable level of magnetic-field intensity was observed inside the sphere, showing that the PEC model was actually inaccurate, at least considering the near-zone characteristics.

Figure 2 next presents the results when the real part of the permittivity was negative at 10 THz. We noted that negative real permittivity led to an increased imaginary part of the wavenumber, leading to a fast decay of fields, even more than did metallic losses. The magnetic-field intensity was more confined in the vicinity of the surfaces in first three cases, i.e., when the real part was –20000. Interestingly, despite the magnetic-field intensity significantly depending on the permittivity, the electric-field intensity was almost the same (and very small) for all cases, including the PEC case. In fact, the decay rate was the same for the electric-field intensity and the magnetic-field intensity. However, very small intrinsic impedance values further suppressed the electric-field intensity, making it vanishingly zero in all cases. This also led to vanishingly small power-density values, making the penetrable particles behave like PEC.

Figure 3 depicts the cases when the real permittivity took negative values while the frequency was 1 THz. Decreasing the frequency, the spheres became electrically smaller. Consequently, in the last two cases, there was not any visible decay in the magnetic-field intensity due to the very small electrical size of the spheres in comparison to the skin depth. Specifically, the particles became magnetically invisible. Some variation was still seen in the first three cases, since the magnetic-field intensity decayed very quickly with the distance for the given permittivity values in these cases. In all results, the electric-field intensity (and hence the power density) was again vanishingly zero inside the spheres due to the very small intrinsic impedance values.

4. References

1. P. B. Johnson and R.-W. Christy, "Optical Constants of the Noble Metals," *Phys. Rev. B*, **6**, 12, December 1972, pp. 4370-4379.

2. U. Hohenester and J. Krenn, "Surface Plasmon Resonances of Single and Coupled Metallic Nanoparticles: A Boundary Integral Method Approach," *Phys. Rev. B.*, **72**, 195429, November 2005.

3. T. Sondergaard, "Modeling of Plasmonic Nanostructures: Green's Function Integral Equation Methods," *Phys. Status Solidi B.*, **244**, 10, October 2007, pp. 3448-3462.

4. A. M. Kern and O. F. J. Martin, "Surface Integral Formulation for 3D Simulations of Plasmonic and High Permittivity Nanostructures," *J. Opt. Soc. Am. A.*, **26**, 4, April 2009, pp. 732-740.

5. B. Gallinet and O. F. J. Martin, "Scattering on Plasmonic Nanostructures Arrays Modeled with a Surface Integral Formulation," *Photonics and Nanostructures – Fundamentals and Applications*, **8**, 4, September 2010, pp. 278-284.

6. R. Rodriguez-Oliveros and J. A. Sanchez-Gil, "Localized Surface-Plasmon Resonances on Single and Coupled Nanoparticles Through Surface Integral Equations for Flexible Surfaces," *Opt. Exp.*, **16**, 13, June 2011, pp. 12208-12219.

7. Ö. Ergül, "Parallel Implementation of MLFMA for Homogeneous Objects with Various Material Properties," *Prog. Electromagn. Res.*, **121**, November 2011, pp. 505-520.

8. Ö. Ergül, "Fast and Accurate Analysis of Homogenized Metamaterials with the Surface Integral Equations and the Multilevel Fast Multipole Algorithm," *IEEE Antennas Wireless Propag. Lett.*, **10**, November 2011, pp. 1286-1289.

9. M. G. Araujo, J. M. Taboada, D. M. Solis, J. Rivero, L. Landesa, and F. Obelleiro, "Comparison of Surface Integral Equation Formulations for Electromagnetic Analysis of Plasmonic Nanoscatterers," *Opt. Exp.*, **20**, 8, April 2012, pp. 9161-9171.

10. D. M. Solis, J. M. Taboada, and F. Obelleiro, "Surface Integral Equation Method of Moments with Multiregion Basis Functions Applied to Plasmonics," *IEEE Trans. Antennas Propag.*, **63**, 5, May 2015, pp. 2141-2152.

11. H. Gomez-Sousa, O. Rubinos-Lopez, and J. A. Martinez-Lorenzo, "Comparison of Iterative Solvers for Electromagnetic Analysis of Plasmonic Nanostructures Using Multiple Surface Integral Equation Formulations," *J. Electromagn. Waves Appl.*, **30**, 4, February 2016, pp. 456-472.

12. B. Karaosmanoğlu, A. Yılmaz, U. M. Gür, and Ö. Ergül, "Solutions of Plasmonic Structures Using the Multilevel Fast Multipole Algorithm," *Int. J. RF Microwave Comput.-Aided. Eng.*, **26**, 4, May 2016, pp. 335-341.

13. A. Çekinmez, B. Karaosmanoğlu, and Ö. Ergül, "Integral-equation Formulations of Plasmonic Problems in the Visible Spectrum and Beyond," in *Dynamical Systems – Analytical and Computational Techniques*, M. Reyhanoglu (ed.), London, InTech, 2017, pp. 191-214.

14. B. Karaosmanoglu and Ö. Ergül, "Accuracy of the Surface Integral-Equation Formulations for Large Negative Permittivity Values," Proc. Progress in Electromagnetics Research Symp. (PIERS), 2017, pp. 926-933.

15. T. Xia, H. Gan, M. Wei, W. C. Chew, H. Braunisch, Z. Qian, K. Aygün, and A. Aydiner, "An Integral Equation Modeling of Lossy Conductors with the Enhanced Augmented Electric Field Integral Equation," *IEEE Trans. Antennas Propagat.*, **65**, 8, August 2017, pp. 4181-4190.

16. M. Taskinen and P. Ylä-Oijala, "Current and Charge Integral Equation Formulation," *IEEE Trans. Antennas Propagat.*, **54**, 1, January 2006, pp. 58-67.

17. B. Karaosmanoğlu, A. Yılmaz, and Ö. Ergül, "Accurate and Efficient Analysis of Plasmonic Structures Using Surface Integral Equations," *IEEE Trans. Antennas Propag.*, **65**, 6, June 2017, pp. 3049-3057.